Supporting Information

Shilyansky et al. 10.1073/pnas.1004829107

SI Text

Electrophysiology. Whole-cell patch clamp recordings were made in acute slices containing mPFC or striatum. Coronal slices were cut at 350 μM thickness, in modified ACSF containing (in mM) NaCl, 130; KCl, 3; NaH_2PO_4, 1.25; $NaHCO_3$, 26; $MgCl_2$, 5; $CaCl_2$, 1; and glucose, 10. Slices were recovered in standard ACSF (with 2 mM $CaCl_2$ and 2 mM $MgCl_2$) for a minimum of 1 h before recording. Recordings were carried out in a submerged chamber with constant perfusion (2 mL/min) according to standard protocols. Patch pipettes (4–7 Mohm) were filled with cesium methanesulfonate-based electrolyte solution containing (in mM) Cs-methanesulfonate, 130; CsCl, 10; NaCl, 4; $MgCl_2$, 1; MgATP, 5; EGTA, 5; hepes, 10; GTP, 0.5; phosphocreatine, 10; leupeptin, 0.1. Basic membrane properties were measured at the start of each experiment. Spontaneous activity was measured in voltage clamp mode, using continuous recording filtered at 1 kHz. Membranes were voltage-clamped at a potential of −70 mV to record sEPSCs and at a potential of +10 mV to measure sIPSCs. Recordings at both membrane potentials were made in the same cells, allowing measurement of the activity of local excitatory and inhibitory networks onto the same neurons. GABAergic origin of sIPSCs recorded at +10 mV was confirmed by sensitivity to biccuculline (2 μmol), a GABA(A) receptor antagonist. Excitatory origin of sEPSCs recorded at −70 was confirmed by sensitivity to CNQX, an AMPA/KA receptor antagonist, and APV, a NMDA receptor antagonist. When drug applications were carried out, 5-min, drug-free recordings were made, followed by a 7- to 10-min bath perfusion of drug, followed by another 5-min recording in the presence of drug. The last 90 s of each recording were analyzed. Event detection was carried out off-line using MiniAnalysis software. Threshold for event detection was set above the root mean square noise level (usually 10 pA for sIPSCs, 5 pA for sEPSCs). Analysis was carried out blind to genotype.

Biophysical Model. The compartmental model of a layer II/III PFC pyramidal neuron was implemented in the NEURON simulation environment (1) and consisted of five compartments: a soma, an axon, a basal dendrite, a proximal apical dendrite, and a distal apical dendrite, having a total length of 600 μm. The model includes multiple passive and active membrane mechanisms as well as excitatory and inhibitory synaptic mechanisms and was validated against experimental data from cells recorded in this study (Fig. S2). Four pyramidal model neurons were connected in a recurrent circuit that also included one interneuron. The connectivity between the model neurons of the network was based on experimental data (2). Background inhibition and excitation in the model is based on experimental data described within this paper. Persistent activity was induced by providing a synchronous, single pulse stimulation of 40 synapses located on the proximal dendrite of each model pyramidal neuron. The arrangement of synapses within the proximal dendrite varied randomly during 100 repetition trials.

Animal Behavior. The delayed nonmatch to sample task was carried out as a continuous series of self-initiated trials, each consisting of two phases. Briefly, the first phase of each task trial is a sample presentation phase in which one of five horizontally-organized nose-poke apertures is illuminated, with a nose-poke into that aperture being required to progress in the trial. After a correct sample-phase response, a delay ensues, which is then followed by the choice phase in which both the sample and another aperture are illuminated; the mouse must choose the nonmatch aperture to obtain food reinforcement. The sample presentation in phase 1 and the choice response in phase 2 are separated by variable delay periods ranging from 3 to 10 s delays are composed of the sum of an imposed delay in which no apertures were lit and a free delay period in which two apertures were lit but no choice yet made. During training on the nonmatch to sample rule, two WT mice failed to meet the criterion level of 70% correct responding and were subsequently dropped from further testing. During delayed non-match to sample testing with drug administration, one mouse of each genotype was lost to equipment failure.

Human Behavioral Task Paradigms. Participants performed two spatial delayed response tasks, one contrasting maintenance and manipulation of spatial memoranda consisting of arrays of three dots [stMNM (3, 4)], and the other assessing parametrically increasing memory loads [SCAP (2)] consisting of arrays of increasing numbers of dots. Briefly, in the stMNM task, subjects were shown an array of three dots. After the dots disappeared, a cue appeared, indicating to the subject to either hold the array as it was or to flip across the horizontal axis. After a 6-s delay, subjects were shown a probe array of three dots and asked to determine whether they matched the previously shown array (maintenance condition) or the flipped array (manipulation condition). In the SCAP task, an array of one, three, five, or seven dots in different spatial locations was displayed around a central location for 2 s. The subjects were required to maintain the locations over a 3-s delay and then were shown a single probe dot and asked whether or not it was in the location of one of the original probes. Behavioral data were analyzed in SPSS, using repeated measures ANOVA.

Imaging Methods. All scans were acquired on a 3-T Siemens Allegra scanner at the Ahmanson-Lovelace Brain Mapping Center at University of California, Los Angeles, CA. A T2 weighted image with 1.5-mm in-plane resolution was taken for anatomical registration using a set of high-resolution EPI localizers (TR/TE 5000/33 ms, 33 3-mm slices with 1-mm gap, 128 × 128 matrix, 200-mm FOV) in the same AC-PC aligned plane as the functional scans. To match any B0-related distortions, the high-resolution images had readout bandwidth along the phase encoding direction identical to that in the functional scans. Functional slices were matched to those in the T2 weighted image, and used an echo planar (EPI) sequence (TR/TE 3000/45 ms, 90° flip angle, 33 3-mm slices). The SCAP consisted of 180 scans with a duration of approximately 9 min and the stMNM consisted of 256 scans with a duration of 12 min and 45 s.

Functional image analysis was performed using FSL tools (FMRIB's Software Library v3.3; ref. 8). Potential motion artifacts in the EPI data were corrected by using a 3D coregistration (six parameter rigid-body) to register each BOLD image in the time series to the middle data point in the time series. Data were then registered, first the EPI to the subject's individual T2-weighted structural image, then the MNI-152 standard brain (5, 6). Individual subject analyses were carried out using FEAT. Data were spatially smoothed using a 5-mm (FWHM) Gaussian kernel and filtered using a nonlinear high-pass temporal filter with a cut off of 72 s to remove low frequency artifacts. Time-series statistical analysis was carried out using FILM with local autocorrelation correction (7). For the stMNM each condition was modeled and for the SCAP each load was modeled separately in a block design fashion. Motion across the scan was calculated and translation and rotation parameters were entered as covariates to reduce motion related effects. A univariate General Linear Model was applied on a voxel-by-voxel basis so that each voxel's time

course was individually fit to the resulting model, with local autocorrelation correction that was applied within tissue type to improve the estimation of temporal smoothness (7, 8). Goodness-of-fit of each voxel to the models was estimated, and the resulting parameter estimates indicated the degree to which the change in fMRI signal could be explained by each model.

fMRI Statistics. The group analysis was carried out using FLAME (8, 9). Each subject's data from the lower level analysis was entered; variance was estimated separately for patient and control groups to account for different variances between groups. Resulting Z-statistic images were thresholded using clusters determined by $Z > 2.3$ and a (corrected) cluster significance threshold of $P = 0.01$ (10–12). Cluster P values were determined using a spatial smoothness estimation implemented in Feat (5, 12). The ROI analysis was performed in SPSS. To control for the effects of performance, the stMNM voxel-wise fMRI analysis contained only correct trials. In the SCAP, the parametric design enabled the use loads at which performance was nearly matched between groups (80%, load 3, in patients and 84%, load 5, controls). For the SCAP, unpaired t tests were performed between groups. For the stMNM, repeated measures ANOVA were performed.

ROI Analysis. Functionally defined ROI's were created in the MNI-152 standard brain space. In the frontal and parietal lobes, active regions were defined using the conjunction of all subjects and all loads contrasts from each task to allow both groups and tasks to contribute to definition of the ROI. The cluster-thresholded z-statistic image was used, and all contiguous active voxels above the threshold in the region of interest were included in each ROI. For striatal ROIs (caudate and putamen), the Harvard-Oxford structural regions of interest in MNI-152 space were used as structural ROIs. The Featquery (http://www.fmrib.ox.ac.uk/fsl/feat5/featquery.html) program applied the inverse of the transformation matrix from individual to standard space that was generated during the initial registration to warp the ROI's back into each subject's individual space where the statistics were performed. The motion corrected, smoothed, and filtered data across each entire ROI were probed for their percent signal change from baseline.

To assess the relationship between the BOLD activation and working memory performance, a robust regression was performed in Stata (v 8) for each task with functional activation in the right DLPFC predicting accuracy (percent correct). Data were examined for outliers, and subjects with high studentized residuals (>2) were excluded (one patient on each task).

1. Hines ML, Carnevale NT (1997) The NEURON simulation environment. *Neural Comput* 9:1179–1209.
2. Thomson AM, Lamy C (2007) Functional maps of neocortical local circuitry. *Front Neurosci* 1:19–42.
3. Cannon TD, et al. (2005) Dorsolateral prefrontal cortex activity during maintenance and manipulation of information in working memory in patients with schizophrenia. *Arch Gen Psychiatry* 62:1071–1080.
4. Glahn DC, et al. (2002) Maintenance and manipulation in spatial working memory: Dissociations in the prefrontal cortex. *Neuroimage* 17:201–213.
5. Jenkinson M, Smith S (2001) A global optimisation method for robust affine registration of brain images. *Med Image Anal* 5:143–156.
6. Jenkinson M, Bannister P, Brady M, Smith S (2002) Improved optimization for the robust and accurate linear registration and motion correction of brain images. *Neuroimage* 17:825–841.
7. Woolrich MW, Ripley BD, Brady M, Smith SM (2001) Temporal autocorrelation in univariate linear modeling of FMRI data. *Neuroimage* 14:1370–1386.
8. Smith SM, et al. (2004) Advances in functional and structural MR image analysis and implementation as FSL. *Neuroimage* 23 (Suppl 1):S208–S219.
9. Behrens TE, et al. (2003) Non-invasive mapping of connections between human thalamus and cortex using diffusion imaging. *Nat Neurosci* 6:750–757.
10. Worsley KJ, Evans AC, Marrett S, Neelin P (1992) A three-dimensional statistical analysis for CBF activation studies in human brain. *J Cereb Blood Flow Metab* 12: 900–918.
11. Friston K, Worsley K, Frackowiak R, Mazziotta JC, Evans AC (1994) Assessing the significance of focal activations using their spatial extent. *Hum Brain Mapp* 1:214–220.
12. Forman SD, et al. (1995) Improved assessment of significant activation in functional magnetic resonance imaging (fMRI): Use of a cluster-size threshold. *Magn Reson Med* 33:636–647.

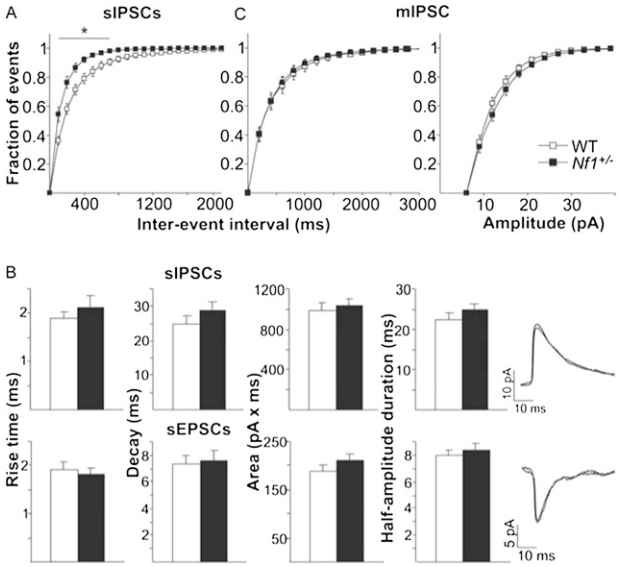

Fig. S1. Frequency of sIPSCs is specifically increased in an activity-dependent manner in the mPFC of *Nf1*$^{+/-}$ mice. (*A*) Cumulative interevent interval (IEI) distribution of sIPSCs is shifted toward shorter IEI in *Nf1*$^{+/-}$ mice ($n = 13$) compared with WT ($n = 16$) (RM ANOVA $P = 0.001$, $^{*}P < 0.05$, Tukey's post hoc). (*B Upper*) Kinetics of sIPSCs in *Nf1*$^{+/-}$ ($n = 9$) and WT ($n = 10$) mice are not different (amplitude $P = 0.58$, rise time = 0.47, area $P = 0.64$, half-width $P = 0.28$, decay $P = 0.24$). (*Lower*) Kinetics of sEPSCs in *Nf1*$^{+/-}$ ($n = 12$) and WT ($n = 12$) mice are not different (amplitude $P = 0.09$, rise time = 0.73, area $P = 0.08$ half-width $P = 0.37$, decay $P = 0.57$). (*Right*) Overlaid representative average sIPSCs (*Upper*) and sEPSCs (*Lower*) from *Nf1*$^{+/-}$ and WT cells. (*C Left*) Cumulative distribution of interevent intervals of mIPSCs in the presence of TTX to block action potential generation in *Nf1*$^{+/-}$ ($n = 10$) and WT ($n = 9$) cells. No difference is seen between genotypes (RM ANOVA $P = 1$) in the absence of action potentials. (*Right*) Cumulative amplitude distribution of mIPSCs recorded from mPFC of *Nf1*$^{+/-}$ ($n = 10$) and WT ($n = 9$) mice are not significantly different (RM ANOVA $P = 0.585$).

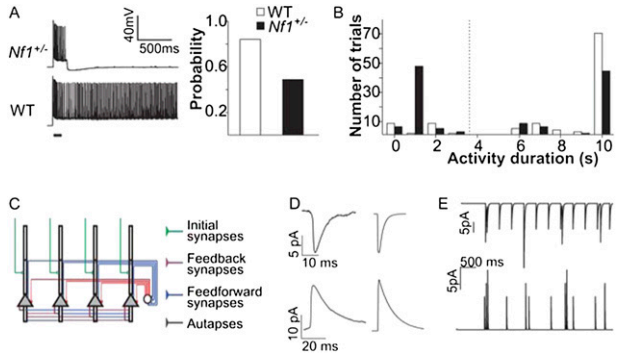

Fig. S2. Increasing synaptic inhibition to levels seen in *Nf1*$^{+/-}$ cells decreases persistent activity in a biophysical model of a prefrontal microcircuit. (*A Left*) Representative trial showing the response of a single cell to stimulation (horizontal line) within the microcircuit. Persistent activity beyond the stimulus is induced in WT, whereas activity is only briefly sustained in the *Nf1*$^{+/-}$ circuit. (*Right*) Probability of persistent activity induction in the *Nf1*$^{+/-}$ microcircuit is decreased compared with WT across 100 trial repetitions. (*B*) Histogram of lengths of sustained activity generated in the *Nf1*$^{+/-}$ and WT microcircuit. Persistent activity was defined as being sustained for more than 3 s (dotted line). *Nf1*$^{+/-}$ microcircuit shows more trials with failure to sustain activity for longer than 1 s. (*C*) Schematic of model network. (*D* and *E*) Validation of the model network. (*D*) Comparison of currents generated by the model (*Right*) and a representative average current we recorded from a WT cell in vitro (*Left*) for EPSCs (*Upper*) and IPSCs (bottom). (*E*) Example spontaneous synaptic excitatory (*Upper*) and inhibitory (*Lower*) currents generated by the model. sEPSCs and sIPSCs shown are generated at a frequency equal to average frequencies recorded from WT mice.

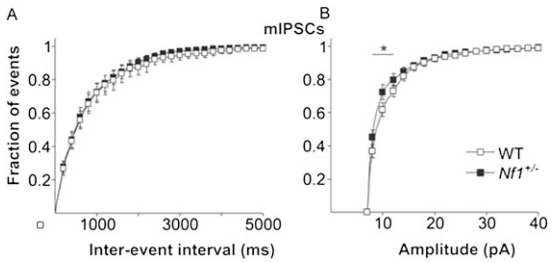

Fig. S3. Striatal neurons show activity dependent increase in frequency and activity independent decrease in amplitude of inhibitory currents. (*A*) Cumulative distribution of interevent intervals of mIPSCs in the presence of TTX to block action potential generation in *Nf1*$^{+/-}$ (n = 9) MSNs and WT (n = 9). No difference is seen between genotypes (RM ANOVA P = 1) in the absence of activity. (*B*) Cumulative amplitude distribution of mIPSCs recorded from striatum show a shift to smaller amplitudes in *Nf1*$^{+/-}$ (n = 9) compared with WT (n = 9) mice (RM ANOVA P = 0.008, *P < 0.05, Tukey's post hoc).

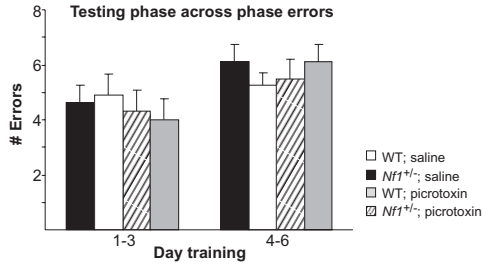

Fig. S4. Specificity of picrotoxin effects on within-phase errors in *Nf1*$^{+/-}$ mice during the delayed win-shift radial arm maze. The dose of picrotoxin used does not affect across phase errors in either *Nf1*$^{+/-}$ or WT mice during the first 6 d of the task (RM ANOVA drug × genotype × day × error P = 0.184). Comparisons made across four groups: saline (n = 20)- and picrotoxin (n = 18)-treated *Nf1*$^{+/-}$ mice and saline (n = 20)- and picrotoxin-treated WT mice (n = 19).

Table S1. Demographics of participants in behavioral and fMRI experiments examining working memory

	NF1 individuals	Controls
Age: mean (SD)	24.00 (4.93)	22.58 (4.56)
Sex: male/female	6/8	5/7
Years education: mean (SD)	14.21 (2.13)	14.88 (2.25)
Handedness: (right/left/other)	13/0/1	11/1/0
Race/ethnicity: (Caucasian/Hispanic/African-American/Asian/Other)	7/5/0/2/0	5/2/2/0/2

Both NF1 and control groups had comparable demographics.

Table S2. Standard neuropsychological battery

Measure	Patients (mean ± SD)	Controls (mean ± SD)
WASI vocabulary	49.91 ± 5.96	60.22 ± 7.64
WASI matrix reasoning	22.08 ± 3.88*	29.11 ± 3.79*
WASI full-scale IQ estimate	88.58 ± 8.14*	111.00 ± 9.04*
CVLT-II trials 1–5 total	51.50 ± 11.35	53.00 ± 8.96
CVLT-II short delay free recall	10.75 ± 3.07	11.56 ± 3.71
CVLT-II long delay free recall	11.42 ± 3.14	12.78 ± 2.68
CVLT-II total intrusions	3.25 ± 3.27	1.78 ± 3.87
WAIS-III digit span forward	9.08 ± 2.55	10.78 ± 1.56
WAIS-III digit span backward	4.83 ± 2.10	6.56 ± 1.59
Trail making A test, s	27.83 ± 18.87	25.40 ± 8.96
Trail making B test, s	68.76 ± 40.14	68.67 ± 26.73
WMS logical memory-I recall	37.08 ± 10.34	46.22 ± 11.80
WMS logical memory-II recall	22.08 ± 8.85	29.56 ± 7.52
WMS spatial span forward	8.17 ± 2.26	9.67 ± 2.29
WMS spatial span backward	6.67 ± 2.05	7.89 ± 2.20

Neuropsychological test data for 12 NF1 patients and nine controls.
*Significant difference P < 0.05, t test.